Received: 13 March 2020 | Revised: 19 May 2020 | Accepted: 21 June 2020

DOI: 10.1002/suco.202000156

TECHNICAL PAPER

fib CEB-FIP WILEY

Cracking behavior of basalt fibre reinforced polymer-reinforced concrete: An approach for the determination of crack spacing and crack width

Sebastian Hofmann | **Ngoc Linh Tran** | **Tilo Proske** | **Carl-Alexander Graubner**

TU Darmstadt, Institute of Concrete and Masonry Structures, Darmstadt, Germany

Correspondence
Sebastian Hofmann, TU Darmstadt, Institute of Concrete and Masonry Structures, Franziska-Braun-Str. 3, 64287 Darmstadt
Email: hofmann@massivbau.tu-darmstadt.de

Abstract

The limitation of the crack width is of central importance for the design in the serviceability limit state. For FRP-reinforced concrete members, the crack width has to be limited for service condition in use and not due to corrosion protection. In this paper, an experimental program of pull-out tests and slender concrete cylinders with basalt fiber-reinforced polymer rebars under centric tension load is presented. The used basalt fiber-reinforced polymer rebars are sand coated and have in addition a helically wrapped thread for a decent profiling. Equations to calculate crack spacing and crack width of FRP-reinforced concrete is derived and calibrated with the obtained experimental results. Finally, the equations are verified with experimental data from other authors and a crack model is given for reinforced concrete members with FRP rebars with a helically wrapped and sand coated surface.

KEYWORDS

FRP, BFRP|, crack spacing, crack width, bond behavior, crack model

1 | INTRODUCTION

The crack widths are of particular interest for the design of reinforced concrete members in the serviceability limit state, where the deformation of the concrete member is directly related to the crack widths, which have to be limited to prevent corrosion of the steel reinforcement. When using non-metallic reinforcement, the carbonation and chloride-induced corrosion of the reinforcement can be neglected. The crack width limitation, for example, in building construction in the serviceability limit state, should be dimensioned to satisfy aesthetic requirements and secure the service conditions. Some of the existing guidelines (e. g.[1,2]) for the design of fiber-reinforced polymer (FRP)-reinforced concrete structures allow a maximum crack width (w_{cr}) between 0.5 mm $\leq w_{cr} \leq$ 0.7 mm. In contrast to many published studies on the flexural deflection performance (e.g., [3–7]), there is still a demand for research on the cracking behavior of FRP-reinforced concrete members.

Not only the mechanical properties are different compared to steel reinforcement, but also the surface shape of FRP rebars are dependent on the applied manufacturer and the manufacturing process. The different shapes can be classified in the following four different categories: plain, sand coated, helically wrapped (and sand coated), and

Discussion on this paper must be submitted within two months of the print publication. The discussion will then be published in print, along with the authors' closure, if any, approximately nine months after the print publication.

This is an open access article under the terms of the Creative Commons Attribution-NonCommercial-NoDerivs License, which permits use and distribution in any medium, provided the original work is properly cited, the use is non-commercial and no modifications or adaptations are made.
© 2020 The Authors. Structural Concrete published by John Wiley & Sons Ltd on behalf of International Federation for Structural Concrete

FIGURE 1 Close up of the investigated BFRP rebars

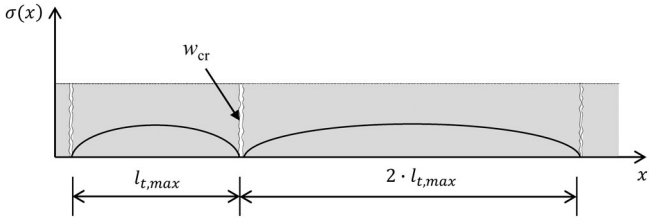

FIGURE 2 Illustration of transfer length on cracked concrete

deformed surfaces (e.g., milled). At the beginning of the research on FRP reinforcement (e.g., [8,9]), it was shown, that the surface shape of FRP rebars has a high influence on the bond behavior between concrete and reinforcement and at the same time on the cracking patterns. To take the different aforementioned material and surface properties into account, the established design formulas for crack spacing and crack width have to be adjusted. In some approaches (e.g.,[10]), design proposals for cracking were calibrated with the help of empirical correction factors on large scale beam tests. The goal of the research presented in this paper is to develop a crack model, which considers the correct material and surface properties on a meso level and uses it as input parameter for a mechanically based crack equation.

In the following sections, the current state of knowledge and theoretical background of the calculation of crack spacings, crack widths and the existing design code models are presented and evaluated with regard to the adjustments for the special material, surface, and bond properties of FRP reinforcement. For the derivation of a crack prediction formula, an experimental program with the focus on the bond conditions and crack spacings of FRP-reinforced concrete members was conducted. The used rebars are made of basalt fibers and epoxy resin, and can be called "basalt fiber reinforced polymer" (BFRP). The surface shape of these rebars can be described as helically wrapped (to gain a slight profiling) in combination with a sand coating (see Figure 1).

To investigate the bond stress–slip relation of the used BFRP rebar, in total, 31 pull out tests according to RILEM[11] with a varying bond length, concrete strength, and bar diameters were carried out and documented. In addition, five centric tension tests on reinforced concrete cylinders were performed to investigate the crack spacing and crack widths under several load levels. With the obtained results, an approach to calculate crack spacing and crack width is finally presented. The developed crack model is based on a mechanical model, which only needs few empirical input parameters to describe the bond stress–slip relation on a meso level and can easily be transferred to other reinforcement types (e.g., GFRP) as well, which have similar surface conditions.

2 | THEORETICAL BACKGROUND

2.1 | Crack spacing and crack width of reinforced concrete

The current Model Code 2010[12] proposes an equation to calculate the mean crack spacings $s_{cr,\,m}$ as follows:

$$\begin{aligned} s_{cr,m} &= 1.5\cdot\left(c+\frac{f_{ctm}\cdot\varnothing}{4\cdot\tau_{bm}\cdot\rho_{eff}}\right) \\ \tau_{bm} &= 1.8\cdot f_{ctm} \end{aligned} \tag{1}$$

with c as concrete cover, $\rho_{eff} = A_{l/Ac,\ eff}$ and $A_{c,\ eff} = \min\,[2.5\cdot(h-d);\ h/2]\cdot b$. This model was developed and calibrated for steel-reinforced concrete.

The presented model is based on the assumption of a constant bond stress distribution along the reinforcement bar and considers the occurring bond stresses in longitudinal direction of the reinforcement until the sum of the bond stress over the transfer length $l_{t,\,max}$ reaches the tensile strength of the concrete. At this local spot, a crack in the concrete member will occur. With this idea of a crack model (see Figure 2), the occurring cracks can have spacing values between the transfer length $l_{t,\,max}$ or $2\cdot l_{t,\,max}$. The reason for this can be explained with the scatter of the concrete's mechanical properties. For the minimum crack spacing $s_{cr,\,min} = l_{t,\,max}$, the concrete has a rather low tensile strength at this local spot, while for the maximum crack spacing $s_{cr,\,min} = 2\cdot l_{t,\,max}$, the concrete tensile strength is just not exceeded (see Figure 2).

To calculate the crack width within a design concept, the worst case has to be considered. The occurring crack width can be calculated according to Model Code 2010[12] as follows:

$$w_{cr,max} = s_{cr,max}(\varepsilon_{lm}-\varepsilon_{cm}) \tag{2}$$

and can be rewritten with the help of the equilibrium of strains and tensions with a stress distribution factor β_t according to Figure 3 as:

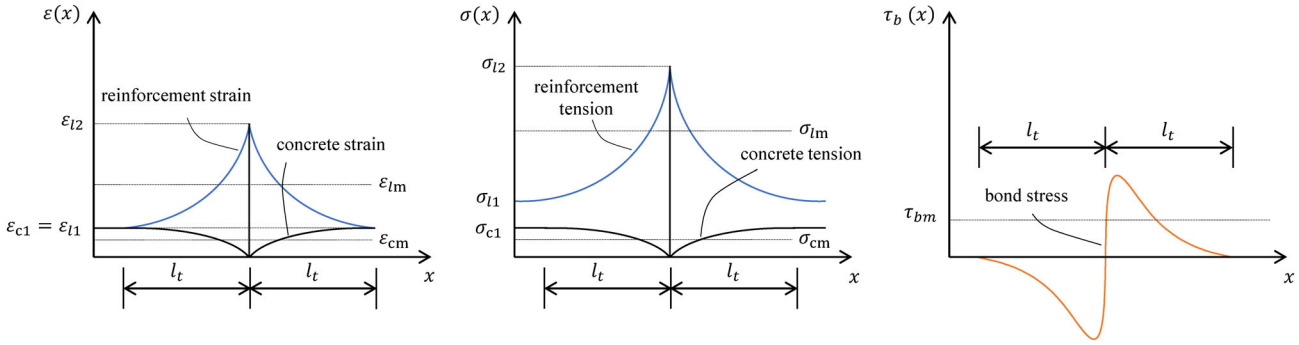

FIGURE 3 Strain and tension distribution at a crack

TABLE 1 Comparison of experimental crack spacing vs. calculated according to MC 2010

Authors	Number of tests	Modulus of elasticity in GPa	Surface condition	Mean $s_{cr,m}$(calc/exp)	CoV
Hofmann et al.[15]	6	53	Helically wrapped + sand coated	1.47	0.15
Issa et al.[16]	4	51–53		1.02	0.19
Elgabbas et al.[17]	5	44.4–48.7		1.64	0.12
All				1.33	0.21

$$w_{cr,max} = s_{cr,max} \cdot \frac{1}{E_l}\left[\sigma_{l2} - \beta_t \cdot \frac{f_{ctm}}{\rho_{eff}} \cdot \left(1 + \frac{E_l}{E_c} \cdot \rho_{eff}\right)\right] \quad (3)$$

With the help of Figure 3, we can describe the equilibrium of stresses at a crack as follows:

$$\sigma_c(x) = \sigma_{c1} - \frac{U_l}{A_c} \cdot \int_0^x \tau_b(\tilde{x}) d\tilde{x} \quad (4)$$

with U_l as reinforcement perimeter and A_c as the concrete cross section area.

2.2 | Determination of crack spacing in FRP-reinforced concrete members

The adaption for FRP reinforcement of the above-presented crack model does not allow to consider the different material properties, such as the much lower modulus of elasticity or surface geometries which leads to a divergent bond behavior. If the modulus of elasticity of the reinforcement is rather low, it comes in range of the modulus of elasticity of the concrete, which brings the strains due to loading closer together. The bond behavior between reinforcement and the embedding concrete has a significant influence on the cracking behavior. According to fib Bulletin 10,[13] numerous parameters (e.g., concrete strength, rebar diameter, surface profiling and modulus of elasticity) have a direct influence on the bond behavior between reinforcement and concrete. Although Model Code 2010[12] does contain a bond stress-slip model for FRP-reinforced concrete, which was developed by Cosenza et al.,[14] it does not provide a general formula to estimate bond stresses for the different existing FRP surface geometries. It is necessary to determine input parameters through experimental investigations on various samples to use this model adequately.

TABLE 2 Mechanical properties of the BFRP reinforcement

	Ø = 6 mm	Ø = 8 mm	Ø = 10 mm
f_{lu} in MPa	≈1,100	≈1,000	≈950
E in GPa	≈56	≈53.5	≈50
$Ø_{mean}$ in mm	5.2	7.3	9.3

Since the different properties of FRP compared to steel rebars cannot be considered accurately, the design model of Equation (1) does not provide precise values for the calculation of the crack spacings and therefore crack widths as well. To show this lack of accordance, the following Table 1 consists of experimental test data of beam tests with similar BFRP reinforcement (helically wrapped and sand coated) as described in Section 1.

This example demonstrates that the calculated values show a large discrepancy in the experimental values, especially the mean values. This clarifies the need of a cracking model, which includes the varying material properties of FRP reinforcement.

The crack width is composed on the one hand of the elongation of the rebar and on the other hand of a relative displacement between the embedding concrete and the rebar, which is called slip. For the serviceability limit state, only crack widths up to 0.7 mm (only for FRP RC components) are relevant (see Section 1), which results in slip values on each side of the crack edges of only $s \leq 0.35$. With this idea of a crack model, we can state that for these low slip values the maximum bond stress is not reached yet. This means we are located on the ascending branch of the bond stress-slip relation (see in Figure 6, the gray marked section). By using this approach, the bond stress distribution can be described as the product of the maximum bond stress and the function of the slip as follows:

$$\tau_b(x) = \tau_{\mathrm{b,max}} \cdot f(s(x)) \tag{5}$$

The resulting slip between reinforcement and concrete is defined with Equation (6).

$$ds(x) = [\varepsilon_1(x) - \varepsilon_c(x)]dx \tag{6}$$

with ε_l = reinforcement strain, ε_c = concrete strain and can be also written as:

$$\frac{ds(x)}{dx} = \frac{\sigma_l(x)}{E_l} - \frac{\sigma_c(x)}{E_c} = \frac{1}{E_l}[\sigma_l(x) - \alpha_l \cdot \sigma_c(x)] \tag{7}$$

Through double differentiation and transformation with $\alpha_l = E_c/E_l$, $U_l/A_l = 4/\varnothing_l$ and $A_c = A_l/\rho_{l,\,\mathrm{eff}}$, the differential equation of the slip is described as:

$$\frac{d^2s(x)}{dx^2} = \frac{4 \cdot (1 + \alpha_l \cdot \rho_{\mathrm{eff}})}{E_l \cdot \varnothing_l} \tau_{\mathrm{b,max}} \cdot f(s(x)) \tag{8}$$

The slip is a relative displacement between the reinforcement and the embedding concrete, and can be described as a form of friction. To solve this differential equation, we can mathematically express the slip as a power function with an integration constant C and the exponent α as follows:

$$f(s(x)) = C \cdot s^{\alpha}(x) \tag{9}$$

with the boundary conditions $s\,(0) = 0$ and $s'(0) = 0$. If we now put the power function into (8), the solution of the slip can be expressed as follows[18]:

$$C \cdot s^{\alpha}(x) = C \cdot \left[\frac{2(1-\alpha)^2(1 + \alpha_l \cdot \rho_{\mathrm{eff}})}{(1+\alpha) \cdot E_l} \cdot \frac{C \cdot \tau_{\mathrm{b,max}}}{\varnothing_l} \cdot x^2 \right]^{\frac{\alpha}{1-\alpha}} \tag{10}$$

With this expression, it is possible to describe the distribution of the bond stress (Equation (5)), which makes the expression of the concrete stress (Equation (4)) solvable. Only the constant of integration C has to be determined.

Finally, the concrete stress curvature in Figure 3 can be described by substituting Equation (10) into Equation (4):

$$\sigma_c(x) = \sigma_{c1} - \frac{4(1-\alpha) \cdot \rho_{\mathrm{eff}}}{1+\alpha} \left[\frac{2(1-\alpha)^2 \left(1 + \alpha_l \cdot \rho_{\mathrm{eff}}\right)}{(1+\alpha) \cdot E_l} \right]^{\frac{\alpha}{1-\alpha}} \cdot \left(\frac{C \cdot \tau_{\mathrm{b,max}}}{\varnothing_l} x^{1+\alpha} \right)^{\frac{1}{1-\alpha}} \tag{11}$$

With the boundary conditions $\sigma_c(l_{t,\ \mathrm{max}}) = 0$ and $\sigma_{c1} = f_{\mathrm{ctm}}$, implying that the tension of the concrete has to be equal to zero at an occurring crack we can solve Equation (11) and find $l_{t,\ \mathrm{max}}$ as follows:

$$l_{t,\mathrm{max}} = \left(\frac{f_{\mathrm{ctm}}}{K} \cdot \frac{1}{\rho_{\mathrm{eff}}} \right)^{\frac{1-\alpha}{1+\alpha}} \left(\frac{\varnothing_l}{C \cdot \tau_{\mathrm{b,max}}} \right)^{\frac{1}{1+\alpha}} \tag{12}$$

with

$$K = \frac{4(1-\alpha)}{1+\alpha} \left[\frac{2(1-\alpha)^2(1 + \alpha_l \cdot \rho_{\mathrm{eff}})}{(1+\alpha) \cdot E_l} \right]^{\frac{\alpha}{1-\alpha}} \tag{13}$$

With the model of concrete cracking in Figure 2, the mean crack spacing can now be calculated. If the concrete properties are symmetrically distributed, the crack spacing can vary in between the two boundaries, $l_{t,\ \mathrm{max}} \leq s_{\mathrm{cr,\ m}} \leq 2 \cdot l_{t,\ \mathrm{max}}$ and can be expressed as follows:

$$s_{\mathrm{cr,m}} = 1.5 \cdot \left(\frac{f_{\mathrm{ctm}}}{K} \cdot \frac{1}{\rho_{\mathrm{eff}}} \right)^{\frac{1-\alpha}{1+\alpha}} \left(\frac{\varnothing_l}{C \cdot \tau_{\mathrm{b,max}}} \right)^{\frac{1}{1+\alpha}} = 1.5 \cdot l_{t,\mathrm{max}} \tag{14}$$

A detailed derivation of these equations and more background information can be found in Tran.[18] The final expression to describe the mean crack spacing according to Equation (14) clarifies, that crack spacings and simultaneously crack widths are quite dependent on the bond stress—slip exponent α, which may be different for FRP reinforcements with their varying surface

geometries and demands a refinement for such reinforcement types. Furthermore, the constant of integration C of the slip Equation (10) has to be found and validated within the scope of experiments, which are presented in the following Section 3.

3 | MODEL VALIDATION BASED ON EXPERIMENTAL INVESTIGATIONS

3.1 | Material properties

For the experimental investigation, BFRP rebars with the nominal diameters of 6, 8, and 10 mm were used. To determine the mechanical properties, three tensile tests of each diameter were carried out on these rebars while the strain was monitored to evaluate the modulus of elasticity. All mechanical properties are presented in Table 2.

The concrete strength of every specimen type was determined on simultaneously produced cubes with an edge length of 150 mm, which were stored under the same conditions and tested at the same day. The cylindric concrete strength with the conversion of $0.8 \cdot f_{cm,\,cube} = f_{cm,\,cyl}$ is given for each specimen in the following sections.

3.2 | Determination of the bond stress–slip relation in pull-out tests

Model Code 2010[12] defines the bond stress to $\tau_{bm} = 1.8 \cdot f_{ctm}$ and $\tau_{b,\,max} = 2.5 \cdot \sqrt{f_c}$ for bond lengths five times the diameter ($l_b = 5$ Ø). This approach also delivers good matching experimental results for helically wrapped and sand-coated BFRP rebars. Table 3 gives a comparison of experimental ($\tau_{b,\,max,\,exp}$) and calculated ($\tau_{b,\,max,\,cal}$) maximum bond stress for different concrete strengths (f_{cm}) and bar diameters (Ø). Although the maximum bond stresses can be predicted quite good with the existing design models, crack spacings cannot be determined accurately (see Table 1). Due to the low modulus of elasticity and different surface condition of FRP reinforcement, the bond stress during a pull-out test with a bond length of $l_b = 5$ Ø reaches its peak at a relatively high slip value (see Figure 6). For this reason, the bond length of some pull-out tests was set to two times the nominal rebar diameter ($l_b = 2$ Ø). This bond length is much smaller than in usual pull-out tests ($l_b = 5$ Ø) according to RILEM.[11] The idea behind the different consideration is, that for concrete members with high reinforcement ratios or small depths, the resulting crack spacing can be quite close to each other. For this circumstances, it may happen, that the transfer length $l_{t,\,max}$ (see Section 2) can be smaller than the assumed bond length of $l_b = 5$ Ø, what other models are based on. When using the approach of Model Code 2010[12] or Eurocode 2[23] deviations of the calculated crack spacing may result, because the bond stress distribution is not considered realistically.

For the experimental investigation, the test specimens were designed based on RILEM TC[11] and are illustrated in Figure 4. A reinforcement bar was centered in a concrete cube with an edge length of 150 mm (see Figure 4, right). To ensure the desired bond length l_b, the bond between reinforcement bar and concrete is interrupted by using a PVC sleeve (tube) and an appropriate sealing. The concrete cover is sufficiently large due to the selected geometric dimensions to eliminate the failure due to concrete splitting. The pull-out tests were performed with BFRP reinforcement of the nominal diameters of 6, 8, and 10 mm.

The bond stress can be calculated according to Equation (15), where P is the test load, Ø is the mean diameter of the rebar and l_b the bond length.

$$\tau_{bm} = \frac{P}{\tau \cdot \text{Ø} \cdot l_b} \tag{15}$$

To carry out the pull-out tests, all specimens were placed vertically in a tensile testing machine. On the bar end facing away from the load, the occurring slip s_{ue} was documented and recorded using an inductive displacement transducer. The slip s_{le} at the loaded end of the rod was recorded with the help of three inductive displacement transducers on the bottom face of the test specimen. At the same time, the strains in the reinforcement bar were also documented with the help of a strain recording sensor. By knowing the elongation of the bar, the change in length due to loading could be subtracted from the slip measurement at the lower face of the concrete body and the slip at the loaded end of the bar could be determined with the following equation:

$$s_{le,net} = \frac{s_{le,1} + s_{le,2} + s_{le,3}}{3} - \Delta l_{le} \tag{16}$$

The results of all pull-out tests are presented in Table 4. The obtained results show, that with increasing bond lengths, a difference of the bond stresses between the loaded and unloaded end of the rebar may occur, which could be observed in Achillides and Pilakoutas.[24] Furthermore, Shen et al.[25] and Beycioglu and Seis[26] found out that the bond stresses of BRFP rebars are decreasing with increasing bond lengths, which also could be observed here for the presented experimental

TABLE 3 Comparison of experimental and calculated maximum bond stresses

Authors	Ø (mm)	f_{cm} (MPa)	$\tau_{b,\,max,\,exp}$ (MPa)	$\tau_{b,\,max,\,cal} = 2.5 \cdot \sqrt{f_c}$ (MPa)	$\tau_{b,\,max,\,cal}/\tau_{b,\,max,\,exp}$
Hofmann et al.[19]	8	25	12.5	12.5	1.0
	8	43	16.9	16.4	0.97
	8	56	21.9	18.7	0.85
Kampmann et al.[20]	10	51	22.0	17.9	0.81
Wolf et al.[21]	10	42	14.4	16.2	1.13
El Refai et al.[22])	8	50	17.4	17.7	1.02
	10	50	14.5	17.7	1.22
	12	50	17.0	17.7	1.04

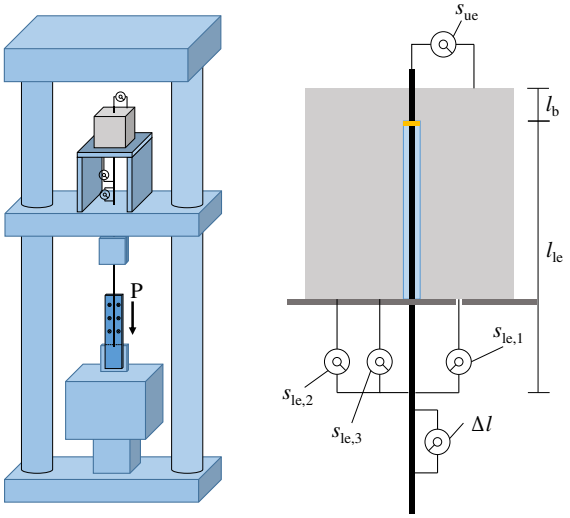

FIGURE 4 Test setup of the pull-out tests

results (see Table 4). The rather short bond length ($l_b = 2$ Ø) was chosen to ensure a constant bond stress distribution, because the shorter the bond length, the more homogenous the acting bond stress can be assumed. As an example, the bond stress–slip diagram of two specimens with an 8 mm rebar is given in Figure 5, which shows the curves of the slip on the loaded and unloaded end of the rebar. Both curves fit well together, justifying the assumption of a constant distribution of bond stresses over a short bond length. In comparison, a specimen with the same configuration, just with a bond length of 10 times the diameter does not show the same results of the unloaded and loaded end slip and confirm the above-mentioned assumption.

In the following diagram (Figure 6), pictures the bond stress–slip relation of the pull-out tests only for the unloaded bar end and a bond length of $l_b = 5$ Ø. The acting bond stresses could be reached for all specimens at a recorded slip of approximately 0.5 mm, where the increase of the bond strength is flattening almost horizontally.

To describe the ascending branch of the bond stress–slip relation according MC 2010 (see Equation (9)) the exponent α has to be determined. As shown in Hofmann et al.,[19] the exponent is directly dependent on the concrete strength and it is within the range of ($0.3 \leq \alpha \leq 0.4$) for normal concrete. The bond stress–slip relation of the here performed experiments could confirm this above-mentioned assumption (see Figure 6).

The bond stress–slip relation can be calculated with the following equation according to the well-known model of Eligehausen et al.[27]:

$$\tau_b(s) = \tau_{b,max} \cdot \left(\frac{s}{s_1}\right)^{\alpha} \tag{17}$$

The exponent α could be found by using a numerical solver, which adjusts the parameter α until the area of the bond stress–slip–curve of the experimental data and the model according to Equation 17 are equal to each other for a slip value up to $s_1 = 0.5$ mm. For the investigated specimens, the exponent was within a range of $0.28 \leq \alpha \leq 0.43$. For higher concrete strengths, the exponent α tends to lower values and increases for lower concrete strengths. This circumstance is easily to see, if we compare the normalized bond stresses in Figure 6 (right). The diagram shows the course of acting the bond stress τ_{bm} divided by the bond stress, which was reached at a slip value of 0.5 mm and clarifies the influence of the concrete strength on the bond stress distribution and therefore the exponent α. To express α depending on the concrete strength, a simplified expression could be found for the investigated FRP reinforcement type as follows:

$$\begin{aligned} \alpha &= 0.5 - \frac{f_{cm}}{280} \\ s_1 &= 0.5 \end{aligned}$$

Furthermore, the maximum bond stress of short bond lengths $l_b \leq 2$ Ø is significantly higher than for usual

TABLE 4 Experimental results of all pull-out tests

Specimen notation	$\tau_{bm,\,max}$	$\tau_{bm,\,max}/\sqrt{f_{cm}}$	$\tau_{bm}(s = 0.5)$	$\tau_{bm}(s = 0.5)/\sqrt{f_{cm}}$	f_{cm}
	MPa	—	Mpa	—	MPa
P.B6.29.5Ø.#1	14.40	2.67	11.52	2.13	29
P.B6.29.5Ø.#2	15.79	2.93	11.24	2.08	
P.B6.29.5Ø.#3	15.45	2.86	10.73	1.99	
P.B8.29.5Ø.#1	12.71	2.36	11.09	2.05	
P.B8.29.5Ø.#2	13.44	2.49	10.75	1.99	
P.B8.29.5Ø.#3	13.65	2.53	11.15	2.07	
P.B10.29.5Ø.#1	12.36	2.29	11.22	2.08	
P.B10.29.5Ø.#2	12.58	2.33	12.21	2.26	
P.B10.29.5Ø.#3	12.74	2.36	11.81	2.19	
P.B6.44.5Ø.#1	17.82[a]	—	16.69	2.51	44
P.B6.44.5Ø.#2	23.84	3.59	16.25	2.48	
P.B8.44.5Ø.#1	17.80	2.68	16.72	2.52	
P.B8.44.5Ø.#2	15.70[a]	—	14.86 (s = 0.47)	—	
P.B8.44.5Ø.#3	17.45	2.63	15.89	2.42	
P.B10.44.5Ø.#1	17.27	2.60	16.43	2.48	
P.B10.44.5Ø.#2	17.41	2.62	16.21	2.44	
P.B8.57.5Ø.#1	21.87	2.89	19.78	2.61	57
P.B8.57.5Ø.#2	21.42	2.83	18.56	2.45	
P.B8.57.5Ø.#3	20.04[a]	—	18.92	2.50	
P.B10.57.5Ø.#1	19.95[a]	—	17.98	2.38	
P.B10.57.5Ø.#2	20.62	2.73	19.30	2.55	
P.B10.C50.5Ø.#3	14.84[a]	—	—	—	
P.B6.36.2Ø.#1	21.10	3.52	20.84	3.47	36
P.B8.36.2Ø.#1	20.93	3.49	20.81	3.47	
P.B10.36.2Ø.#1	20.86	3.48	20.32	3.39	
P.B10.36.2Ø.#1	21.16	3.63	20.01	3.43	
P.B10.36.2Ø.#2	20.77	3.56	20.59	3.53	
P.B8.36.4Ø.#1	18.67	3.11	16.78	2.80	36
P.B8.36.6Ø.#1	16.31	2.71	14.94	2.49	
P.B8.36.8Ø.#1	16.77	2.80	14.70	2.45	
P.B8.36.10Ø.#1	15.63	2.61	14.23	2.37	

[a]Failure at the anchorage before finishing the complete test program.

bond lengths. Ritter[28] investigated many influence parameters on the bond stresses in the scope of a large experimental program. The results showed an increase of the bond stress of about 40% for specimens with $l_b = 2$ Ø compared to $l_b = 5$ Ø on conventional steel reinforcement. These findings also coincide to the obtained experimental results of the pull-out tests for short bond lengths on the helically wrapped and sand-coated BFRP rebars (see Figure 7 and Table 4). With these results it is possible to describe the maximum acting bond stress for the targeted bond model as follows:

$$\tau_{b,max} = 2.5 \cdot \sqrt{f_{cm}} \cdot 1.4 = 3.5 \cdot \sqrt{f_{cm}} \tag{18}$$

Finally, we can use all obtained experimental data and express the bond stress–slip relation with a simplified equation as:

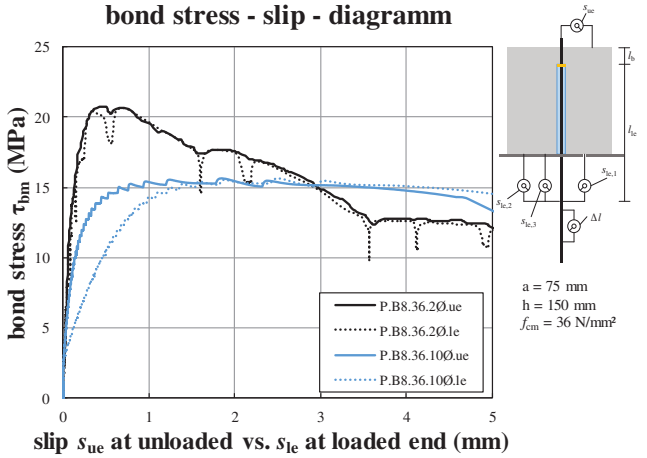

FIGURE 5 Slip at loaded end vs. un loaded end

$$\tau_b(s) = 3.5 \cdot \sqrt{f_{cm}} \cdot \left(\frac{s}{0.5}\right)^{0.5-\frac{f_{cm}}{280}} \text{ for } l_b = 2\,\emptyset$$
$$\tau_b(s) = 2.5 \cdot \sqrt{f_{cm}} \cdot \left(\frac{s}{0.5}\right)^{0.5-\frac{f_{cm}}{280}} \text{ for } l_b = 5\,\emptyset \quad (19)$$

By using the proposed formula of Equation (19) of the bond stress distribution, it is possible to describe the ascending branch of the bond stress–slip–diagram of this type of FRP rebars quite accurately, as shown in the diagram (see Figure 7). When using this approach as a bond model, it can serve as an input parameter to solve the crack development equations presented in Section 2.

3.3 | Determination of the crack spacing in centric tension tests of reinforced cylinders

In the second part of the experimental program, concrete cylinders with one centric rebar were tested under tension load to investigate the crack development and crack spacings. All specimens had the length of 955 mm with varying diameters and a cylindric concrete strength of $f_{cm} = 36$ MPa. The specimen configuration is given in Table 5. The concrete cover is considered small enough to activate the complete concrete cross section to carry tension, which also shows the calculated effective concrete area $A_{c,\,eff}$ in Table 5.

The test setup consisting of the test machine and the specimen itself is shown in Figure 8. Due to the sensitivity against transverse pressure to the FRP reinforcement, an anchorage steel tube had to be attached to secure an unscathed load introduction into the rebar.

During the load application, the total strain of each specimen was recorded with the aid of a displacement transducer, which was attached at both ends of the concrete cylinder. The tension load was applied in displacement-controlled mode with a feed rate of 3.0 mm/min up to a maximum load of approximately 50% of the rebars rupture stress. After that, the test load was completely relieved and the occurred cracks and spacings s_{cr} were documented (see Table 6).

In addition, an exemplary picture of the specimen DK40.B6 as example is shown in Figure 9. The picture was taken after the applied load and illustrates the occurring cracks of the concrete cylinder.

With the obtained experimental results of all tension tests, the equation of mean crack spacing (Equation (14)) can be solved to find the integration constant C through regression analysis. Due to the fact, that rising concrete strengths lead to bond stresses reaching its maximum at lower slip values,[19,29] it is necessary to adjust the parameter C. To not overestimate the expression $C \cdot \tau_{b,\,max}$ in Equation (14), the C value has to be smaller for high and larger for low concrete strengths. For this reason, the parameter C can be expressed as a power function of the slip exponent α, and the corresponding slip value when the nonlinear ascending branch will reach the peak of the bond stress–slip relation. With this approach, the integration constant can be described as follows:

$$C = \left(\frac{1}{s_1}\right)^{\alpha} = B^{\alpha} \quad (20)$$

The parameter B could also be found through regression analysis and should be equal to 2.0 for the assumption of $s_1 = 0.5$ of the presented bond model. The corresponding slip value s_1 can now be calculated and is given in addition to the parameter B in Table 6. The mean value of s_1 of all tension tests was 0.52 mm, which confirms the approach of the bond model of Equation (17). Now all parameters are defined to calculate bond stresses and crack spacings of concrete members with FRP reinforcement with helically wrapped and sand-coated surface conditions.

Finally, the tension stiffening factor β_t needs to be examined to calculate the crack width according to Equation (3). For this reason, a load-strain-diagram is given in Figure 10, where the uncracked state (a), the process of cracking (b) and the postcracking stage with the participation of the concrete in tension (c) is illustrated. The following equation describes the dependencies of strains according to Figure 10:

$$\varepsilon_{Bm} = \varepsilon_{B2} - \beta_t \cdot (\varepsilon_{r2} - \varepsilon_{r1}) \quad (21)$$

With the measured strains taken from the diagram in Figure 10, the contribution of tension stiffening for the investigated specimen can be evaluated to give a factor of $\beta_t = 0.6$, which is similar to steel reinforcement according to Model Code 2010.[12] This obtained test dataset can be

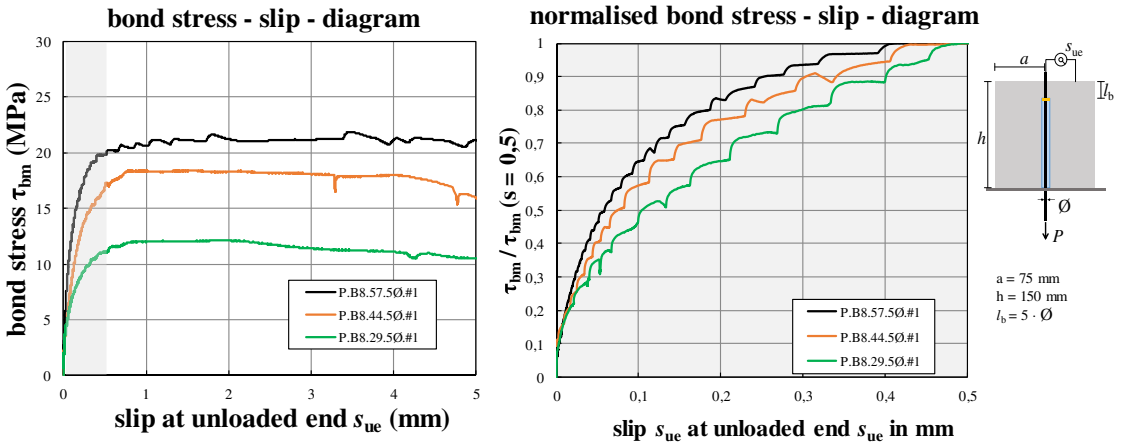

FIGURE 6 bond stress–slip relation of BFRP reinforcement with different concrete strengths (left) and the normalized (τbm/τbm [0.5 mm])bond stress–slip relation (right)

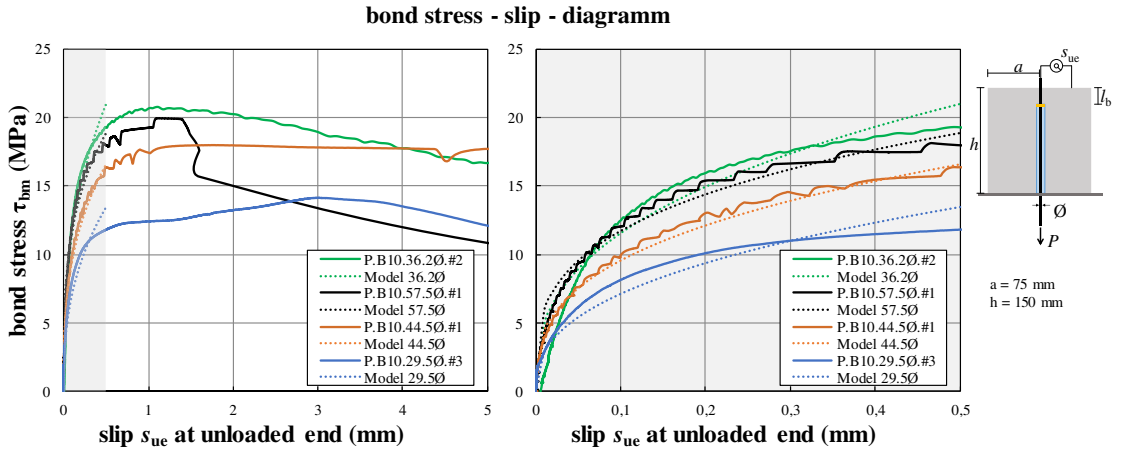

FIGURE 7 Bond stress–slip relation of the pull-out tests compared to the model of Equation (19)

TABLE 5 Specimen configuration for the tension tests

Specimen	$\varnothing_c$(mm)	A_c(mm^2)	$A_{c,\,eff}$(mm^2)	A_{rebar}(mm^2)	$\rho = A_{rebar}/A_c$(%)
DK40.B6	36.4	1,040	1,019	22	2.16
DK75.B10	71.4	4,003	3,935	68	1.72
DK50.B6	46.4	1,690	1,669	22	1.32
DK100.B8	93.6	6,880	6,813	42	1.00
DK125.B10	118.6	11,047	10,979	68	0.62

used to validate the developed crack model, which is presented in Section 4.

4 | APPROACH FOR CRACK SPACING AND CRACK WIDTHS IN FRP-REINFORCED CONCRETE MEMBERS

In Section 2, the derivation of transfer lengths of reinforcement bars in concrete members is presented. The transfer length describes the maximum lengths on which bond stresses can be initiated to the concrete structure until a crack will occur due to the stress exceeding the concrete tensile strength f_{ctm}. With the determination of the transfer length, crack spacing and crack widths can be calculated properly. The obtained parameters α, $\tau_{b,\,max}$ and C of the experimental investigation, presented in section 3, are required as input parameters for the determination of the crack spacing Equation (14):

$$s_{cr,m} = 1.5 \cdot l_{t,max} = 1.5 \cdot \left(\frac{f_{ctm}}{K} \cdot \frac{1}{\rho_{eff}} \right)^{\frac{1-\alpha}{1+\alpha}} \left(\frac{\varnothing_l}{C \cdot \tau_{b,max}} \right)^{\frac{1}{1+\alpha}}$$

with

$$\alpha = 0.5 - \frac{f_{cm}}{280}$$

$$\tau_{b,max} = 3.5 \cdot \sqrt{f_{cm}}$$

$$C = 2.0^{\alpha}$$

To verify the new model, experiments from other publications are used in which a similar reinforcement (helically wrapped and sand coated) was used and the crack spacing was documented. These tests are summarized in Table 7 and compared to the calculated crack spacing according to Equation (14). The mean value of 1.04 and the associated standard deviation of 0.11 show, that the new model achieves very good results for calculating the average crack spacing.

Since the crack spacing can be determined precisely, it is also possible to calculate the maximum crack width for the stabilized crack stage according to the mechanically based model, presented in Section 2 (Equations (2) and (3)); as follows:

$$w_{cr,max} = s_{cr,max} \cdot \frac{1}{E_l} \left[\sigma_{12} - \beta_t \cdot \frac{f_{ctm}}{\rho_{l,eff}} \cdot \left(1 + \frac{E_l}{E_c} \cdot \rho_{eff} \right) \right]$$

with $\beta_t = 0.6$ for short-term loading; $s_{cr,\,max} = 2 \cdot l_{t,\,max}$ and $\sigma_{l,\,2}$ as the reinforcement tension due to loading on the concrete member.

In conclusion, it must be emphasized that the presented approach in this work is based on a bond model with a maximum slip value of 0.5 mm. This means only crack widths up to $w_{cr,\,max} \leq 1.0$ mm can be determined reliably, which is sufficient for the design of the serviceability limit state, in which crack widths smaller than 0.7 mm must be achieved.

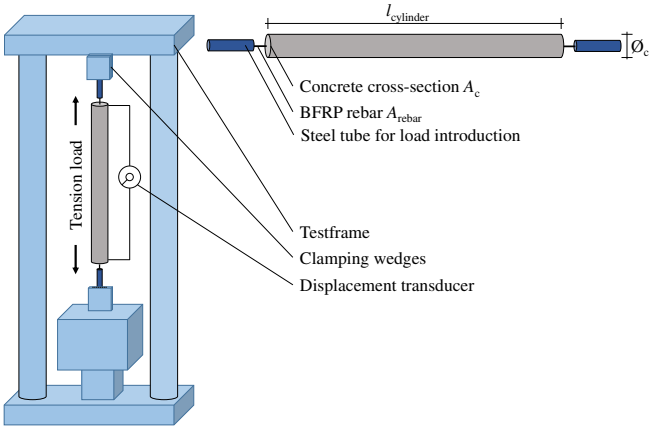

FIGURE 8 Test setup of the tension tests on concrete cylinders

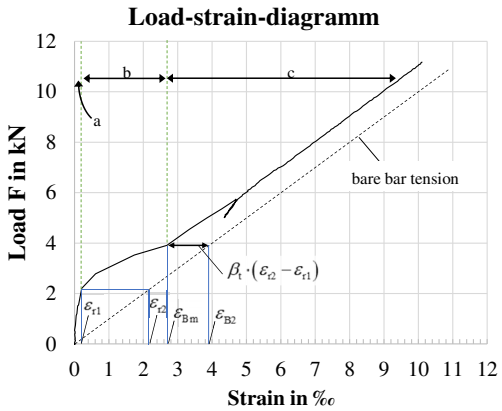

FIGURE 10 Load-strain-diagram of Specimen DK40.B6

TABLE 6 Experimental results of the tension tests

Specimen	DK40.B6	DK75.B10	DK50.B6	DK100.B8	DK125.B10	Mean
$s_{cr,\,m}$	61.8	105.7	93.6	108.1	182.0	—
C	1.34	1.23	1.06	1.37	1.34	1.268
B	2.203	1.752	1.171	2.290	2.160	1.915
s_1	0.45	0.57	0.85	0.44	0.46	0.52

FIGURE 9 Cracked specimen DK40.B6 after the tension test

TABLE 7 Comparison of experimental crack spacing vs. calculated crack spacing

Authors	Notation	f_{cm} (MPa)	$\varnothing_l$ (mm)	E_l (GPa)	f_{ctm} (MPa)	ρ_{eff} (%)	$s_{cr,m,cal}$ (mm)	$s_{cr,m,exp}$ (mm)	Cal/exp
Bending tests									
Hofmann et al.[15]	V01B	33	7.3	53.5	2.88[a]	0.89	146.0	150	1.03
	V02B	36	7.3	53.5	3.05[a]	0.89	140.9	134	0.95
	V04B	39	7.3	53.5	3.05[a]	1.75	102.8	117	1.11
	V06B	39	5.2	56.0	3.22[a]	0.47	145.2	124	0.85
	V07B	39	5.2	56.0	3.22[a]	0.94	104.7	113	1.08
	V08B	39	7.3	53.5	3.22[a]	0.89	136.1	131	0.96
Issa et al.[16]	5–10N5	36	10	53.0	3.05[a]	1.82	125.6	117	0.93
	5–13N5	36	13	51.0	3.05[a]	3.02	118.8	125	1.05
	5–16N5	36	16	51.0	3.05[a]	4.67	112.5	139	1.23
	6–16N7	36	16	51.0	3.05[a]	5.64	102.7	111	1.08
Elgabbas et al.[17]	B-2#10	42.5	10	44.4	3.41[b]	0.83	161.4	157	0.97
	B-4#10	42.5	10	44.4	3.41[b]	1.25	132.3	131	0.99
	B-2#12	42.5	12	45.3	3.41[b]	1.19	156.0	168	1.07
	B-4#12	42.5	12	45.3	3.41[b]	1.79	127.8	122	0.95
	B-2#16	42.5	16	48.7	3.41[b]	2.12	148.4	175	1.18
Füllsack-Köditz[30]	B2-HB-LS1	55	12	40.8	4.04[a]	2.18	96.7	95	0.99
	B2-HB-LS2	55	12	40.8	4.04[a]	2.18	96.7	116	1.20
	B2-HB-LS3	55	12	40.8	4.04[a]	2.18	96.7	116	1.20
Tension tests									
Niewels[31]	D-A9-8	32.0	9.0	46.7	2.82[a]	1.13	147.2	140	0.95
All								Mean	1.04
								COV	0.11

[a] $f_{ctm} = 0.3 \cdot (0.9 \cdot f_{cm})^{2/3}$.
[b] provided experimental data.

5 | SUMMARY

In the context of this paper, a theoretical model for the determination of crack spacing and widths for FRP reinforcement with a helically wrapped and sand-coated surface condition is presented. To be able to use this model properly, some input parameters had to be found through experimental investigations, which are presented in Section 3. At first, the bond properties for this type of reinforcement had to be identified and introduced in the context of a bond model. With the obtained experimental data, a bond law for the ascending branch of the bond stress–slip relation could be defined. This bond law serves as an input parameter for the derived crack equations. After that, a total of five tension tests on concrete cylinders were carried out to investigate the cracking behavior under tension load. Within these experiments, the crack spacing was investigated and the crack model, which was developed beforehand, was evaluated and calibrated. Finally, the proposed crack model was validated through various experimental test data of bending and tension tests of other authors. The achieved mean value and standard deviation confirm a thorough result for the developed crack model.

However, the proposed model is calibrated only for FRP reinforcement with a helically wrapped and sand-coated surface condition and concrete strengths up to $f_{cm} = 60$ MPa, but can be extended with the help

of further experimental test data (e.g., other surface conditions and/or higher concrete strengths), when following the presented method above.

NOTATIONS

$A_{c,\,eff}$	effective area of concrete in tension
A_l	cross section area of flexural reinforcement
C	integration value
E_c	modulus of elasticity of the concrete
E_l	modulus of elasticity of the flexural reinforcement
P	test load
Ø	diameter
c	concrete cover
d	structural height of the concrete member
f_{cm}	concrete compression strength
f_{ctm}	concrete tensile strength
f_{lu}	ultimate reinforcement strength
h	total height of the concrete member
l_b	bond length
l_t	transfer length
$l_{t,\,max}$	maximum transfer length
s	slip
$S_{cr,\,m}$	mean crack spacing
$S_{cr,\,max}$	maximum crack spacing
$s_{cr,\,min}$	minimum crack spacing
$w_{cr,\,max}$	maximum crack width
α	bond coefficient
α_l	ratio of the modulus of elasticity between concrete and reinforcement
β_t	tension stiffening factor
ε_{r1}	strain at first crack on composite cross section
ε_{r2}	strain in bare rebar at first crack
ε_{B2}	strain at bare bar after cracking stage
ε_{BM}	strain in composite cross section after cracking stage
ε_{cm}	mean concrete strain
ε_{lm}	mean flexural reinforcement strain
ρ_{eff}	effective reinforcement ratio
σ_c	concrete stresses
σ_l	stress in flexural reinforcement
τ_b	bond stress
τ_{bm}	mean bond stress
$\tau_{b,\,max}$	maximum bond stress

ORCID

Sebastian Hofmann https://orcid.org/0000-0001-7865-6729

REFERENCES

1. ACI 440.1R-15. Guide for the design and construction of structural concrete reinforced with FRP bars. Farmington Hills, MI: American Concrete Institute, 2015.
2. JSCE. Recommendation for design and construction structures using continuous fibre reinforcing materials. Sappro: Japan Society of Civil Engineers, 1997.
3. Cai J, Pan J, Zhou X. Flexural behavior of basalt FRP reinforced ECC and concrete beams. Construct Build Mater. 2017;142:423–430. https://doi.org/10.1016/j.conbuildmat.2017.03.087.
4. Lapko A, Urbanski M. Experimental und theoretical analysis of deflections of concrete beams reinforced with basalt rebar. Archiv Civil Mech Eng. 2014;15(1):223–230. https://doi.org/10.1016/j.acme.2014.03.008.
5. Pawłowski, D., & Szumigała (2015). Flexural behaviour of full-scale basalt FRP RC beams—Experimental and numerical studies. Procedia Eng, 108, 518–525. https://doi.org/10.1016/j.proeng.2015.06.114
6. Pecce M, Manfredi G, Cosenza E. Experimental response and code models of GFRP RC beams in bending. J Compos Constr. 2000;4(4):182–190. https://doi.org/10.1061/(ASCE)1090-0268(2000)4:4(182).
7. Tomlinson D, Fam A. Performance of concrete beams reinforced with basalt FRP for flexure and shear. J Compos Constr. 2015;19(2):4014036. https://doi.org/10.1061/(ASCE)CC.1943-5614.0000491.
8. Hao Q, Wang Y, He Z, Ou J. Bond strength of glass fiber reinforced polymer ribbed rebars in normal strength concrete. Construct Build Mater. 2009;23(2):865–871. https://doi.org/10.1016/j.conbuildmat.2008.04.011.
9. Malvar J. Tensile and bond properties of GFRP reinforcing bars. ACI Mater J. 1995;92(3):276–285. https://doi.org/10.14359/1120.
10. Barris C, Torres L, Vilanova I, Miàs C, Llorens M. Experimental study on crack width and crack spacing for glass-FRP reinforced concrete beams. Eng Struct. 2017;131:231–242. https://doi.org/10.1016/j.engstruct.2016.11.007.
11. RILEM TC, editor. RC 6: Bond test reinforcing steel, 2, pull-out test. London (UK): E & FN SPON, 1983.
12. Fib. Model Code for Concrete Structures 2010. Lausanne, Switzerland: Fédération internationale du betón, 2013.
13. Fib. Bulletin 10–Bond of reinforcement in concrete: State-of-art report. Bulletin/International Federation for Structural Concrete: Vol. 10. Lausanne, Switzerland: Fédération internationale du betón, 2000.
14. Cosenza E, Manfredi G, Realfonzo R. Behavior and modeling of bond of FRP Rebars to concrete. J Compos Constr. 1997;1(2):40–51.
15. Hofmann, S., Tran, N., Proske, T., & Graubner, C.-A. Shear capacity of BFRP reinforced concrete without shear reinforcement: Advances in engineering materials, structures and systems: Innovations, mechanics and applications. *Proceedings of the 7th International Conference on Structural Engineering, Mechanics and Computation* (2019a), pp. 1531–1536.
16. Issa MA, Ovitigala T, Ibrahim M. Shear behavior of basalt fiber reinforced concrete beams with and without basalt FRP stirrups. J Compos Constr. 2016;20(4):4015083. https://doi.org/10.1061/(ASCE)CC.1943-5614.0000638.
17. Elgabbas F, Vincent P, Ahmed EA, Benmokrane B. Experimental testing of basalt-fiber-reinforced polymer bars in concrete beams. Compos Part B Eng. 2016;91:205–218. https://doi.org/10.1016/j.compositesb.2016.01.045.
18. Tran, N. L. (2018). Shear strength of slender reinforced concrete members without shear reinforcement – A mechanical model. Habilitation Thesis. Technische Universität Darmstadt.

19. Hofmann S, Proske T, Graubner C-A. Verbundverhalten besandeter basaltfaserverstärkter Kunststoffbewehrung. Beton- Und Stahlbetonbau. 2019b;380(6):164–522. https://doi.org/10.1002/best.201900076.
20. Kampmann R, Rambo-Roddenberry M, Telikapalli S. Performance evaluation, material and specification development for basalt fiber reinforced polymer (BFRP) Reinforcing bars embedded in concrete. Tallahassee, Florida: Florida Department of Transportation, 2019.
21. Wolf B, Glomb DS, Kustermann A, Dauberschmidt C. Untersuchung des Zug- und Verbundverhaltens von Basaltfaserverstärkter Kunststoff-Stabbewehrung in Beton. Beton- Und Stahlbetonbau. 2019;114(7):454–464. https://doi.org/10.1002/best.201900019.
22. El Refai A, Ammar M-A, Masmoudi R. Bond performance of basalt fiber-reinforced polymer bars to concrete. J Compos Constr. 2015;19(3):4014050. https://doi.org/10.1061/(ASCE)CC.1943-5614.0000487.
23. EN 1992-1-1. Eurocode 2: Design of concrete structures - part 1–1: General rules and rules for buildings. Brussels: CEN European Committee for Standardization, 2010.
24. Achillides Z, Pilakoutas K. Bond behavior of fiber reinforced polymer bars under direct pullout conditions. J Compos Constr. 2004;8(2):173–181. https://doi.org/10.1061/(ASCE)1090-0268(2004)8:2(173).
25. Shen D, Ojha B, Shi X, Zhang H, Shen J. Bond stress–slip relationship between basalt fiber-reinforced polymer bars and concrete using a pull-out test. J Reinforced Plastics Compos. 2016;35(9):747–763. https://doi.org/10.1177/0731684415627504.
26. Beycioglu A, Seis M. Bond performance of basalt fiber-reinforced polymer bars in conventional Portland cement concrete: A relative comparison with steel rebar using the hinged beam approach. Sci Eng Compos Mater. 2015;24(6):24–918. https://doi.org/10.1515/secm-2015-0210.
27. Eligehausen R, Popov EP, Bertero VV. Local bond stress-slip relationships of deformed bars under generalized excitations. Berkeley, CA: College of Engineering of the University of California in Berkeley, 1983.
28. Ritter, L. (2013). Der Einfluss von Querzug auf den Verbund zwischen Beton und Betonstahl. Dissertation Thesis. TU Dresden.
29. Baena Muñoz, M. (2011). Study of bond behaviour between FRP reinforcement and concrete. Dissertation Thesis. Universitat de Girona.
30. Füllsack-Köditz, R. (2004). *Verbundverhalten von GFK-Bewehrungsstäben und Rissentwicklung in GFK-stabbewehrten Betonbauteilen*. *Schriftenreihe des Institutes für Konstruktiven Ingenieurbau, Bauhaus-Universität Weimar: Vol. 1*. Weimar.
31. Niewels, J. (2008). Zum Tragverhalten von Betonbauteilen mit Faserverbundkunststoff-Bewehrung. Dissertation Thesis. RWTH Aachen.

AUTHOR BIOGRAPHIES

Sebastian Hofmann M.Sc.
TU Darmstadt
Institute of Concrete and Masonry Structures
Franziska-Braun-Str. 3
64287 Darmstadt, Germany
hofmann@massivbau.tu-darmstadt.de

Dr.-Ing. Habil. Linh Ngoc Tran
TU Darmstadt
Institute of Concrete and Masonry Structures
Franziska-Braun-Str. 3
64287 Darmstadt, Germany
tran@massivbau.tu-darmstadt.de

Dr.-Ing. Tilo Proske
TU Darmstadt
Institute of Concrete and Masonry Structures
Franziska-Braun-Str. 3
64287 Darmstadt, Germany
proske@massivbau.tu-darmstadt.de

Univ.-Prof. Dr.-Ing. Carl-Alexander Graubner
TU Darmstadt
Institute of Concrete and Masonry Structures
Franziska-Braun-Str. 3|
64287 Darmstadt, Germany
graubner@massivbau.tu-darmstadt.de

How to cite this article: Hofmann S, Tran NL, Proske T, Graubner C-A. Cracking behavior of basalt fibre reinforced polymer-reinforced concrete: An approach for the determination of crack spacing and crack width. *Structural Concrete*. 2020; 21:2178–2190. https://doi.org/10.1002/suco.202000156